RSC Advances

PAPER

View Article Online
View Journal | View Issue

Cite this: *RSC Adv.*, 2026, **16**, 24218

Structure-based design and optimization of cyclic peptide ligands targeting delta-like ligand 3

Xinyan Gao,[ab] Xiaochuan Zha,[ab] Wenhao Liu,[a] Jiale Xie,[a] Jian Gao[c] and Zonghua Luo *[ad]

Received 8th April 2026
Accepted 29th April 2026

DOI: 10.1039/d6ra02966c

rsc.li/rsc-advances

Delta-like ligand 3 (DLL3) is a promising theranostic target due to its high and specific overexpression in small cell lung cancer and other neuroendocrine tumors. To develop novel targeting agents, we designed and synthesized a series of cyclic peptides targeting DLL3. We optimized three key residues: Trp9 and Gly4 on the PepSP1171 core scaffold, and Val4 on PepSP1214, through systematic amino acid substitution and incorporation of non-natural residues. This approach yielded six high-affinity peptides with dissociation constants (K_D) below 100 nM and established an initial structure–activity relationship. The most significant improvement was achieved by substituting Val4 with rigid 1-aminocyclopropanecarboxylic acid, which produced the lead peptide **B5** with a K_D of 12.3 nM. These results validate our rational design strategy and identify peptide **B5** as a promising candidate for the future development of DLL3-targeted theranostic agents.

Introduction

Delta-like ligand 3 (DLL3), characterized as an atypical inhibitory ligand within the Notch signaling pathway, interacts with Notch receptors through its Delta/Serrate/Lag-2 (DSL) domain, leading to the suppression of canonical downstream signaling pathways.[1–3] DLL3 is mainly overexpressed in small cell lung cancer (SCLC) and various neuroendocrine tumors, where its elevated expression correlates with increased tumor aggressiveness, therapeutic resistance, and poor clinical prognosis.[1,4,5] Given its limited expression in normal tissues and overexpression in malignant tumors, DLL3 has emerged as a highly promising target for therapeutic intervention and diagnostic applications.

Therapeutic development targeting DLL3 has primarily focused on several modalities, including antibody-drug conjugates (ADCs), bispecific T cell engagers (TCEs), chimeric antigen receptor T cell (CAR-T) therapies, and radiopharmaceutical treatments (Fig. 1A).[6–9] Although the initial DLL3-targeted ADC, Rovalpituzumab Tesirine (Rova-T), was discontinued due to toxicity concerns and limited clinical efficacy,[10] subsequent next-generation agents such as ZL-1310 and FZ-AD005 have been developed and are currently undergoing clinical evaluation (NCT06179069).[11,12] Tarlatamab (AMG-757), a DLL3-specific TCE that simultaneously binds DLL3 and CD3 to facilitate T-cell-mediated tumor lysis, has advanced into clinical trials with promising antitumor efficacy.[13,14] Preclinical investigations of the DLL3-targeted CAR-T therapy AMG-119 demonstrated potent and specific antitumor activity in SCLC models. A phase I clinical trial (NCT03392064) involving SCLC patients confirmed its safety and tolerability, with favorable cellular kinetics supporting its further investigation in solid tumors.[15] More recently, radiopharmaceutical therapy represents another promising targeted strategy in oncology. The anti-DLL3 antibody SC16, radiolabeled with Lutetium-177, induced complete pathological responses with mild toxicity in patient-derived xenograft models.[7,16] The diagnostic potential of DLL3-targeting was further validated in a Phase I/II clinical study (NCT03392064), wherein [^{89}Zr]Zr-DFO-SC16.56 PET/CT proved safe and feasible in patients with neuroendocrine carcinoma.[17] Additionally, Mariana Oncology Inc. has developed MC-339, a novel DLL3-targeting peptide radioligand therapy utilizing isotopes Lutetium-177 and Actinium-225, intended for the treatment of DLL3-expressing solid tumors.[18]

Collectively, these findings highlight the considerable therapeutic potential of targeting DLL3. Although advancements have been made with macromolecular agents such as antibodies, ADCs, and CAR-T cells, the development of small molecules or peptides targeting DLL3 remains in its early stages, with no peer-reviewed publications available. Cyclic peptides, in particular, offer distinct advantages, including enhanced conformational stability through disulfide or side-chain cyclization, which improves resistance to proteolysis and prolongs half-life. Their relatively small molecular weight (1–3 kDa) enables deep penetration into solid tumors, while

[a]*School of Biomedical Engineering & State Key Laboratory of Advanced Medical Materials and Devices, ShanghaiTech University, Shanghai 201210, China. E-mail: luozh@shanghaitech.edu.cn; Tel: +86-21-20685447*

[b]*School of Life Science and Technology, ShanghaiTech University, Shanghai 201210, China*

[c]*Hangzhou Healthytide Biotechnology Co, Ltd, Hangzhou 310051, China*

[d]*Shanghai Clinical Research and Trial Center, Shanghai 201210, China*

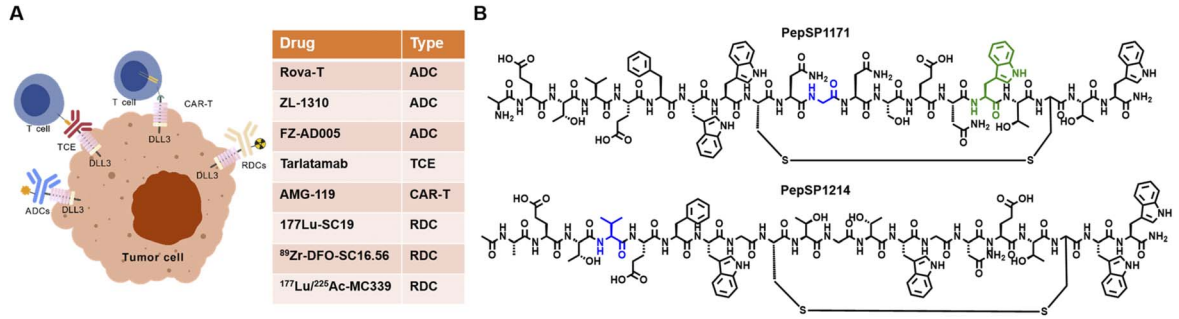

Drug	Type
Rova-T	ADC
ZL-1310	ADC
FZ-AD005	ADC
Tarlatamab	TCE
AMG-119	CAR-T
177Lu-SC19	RDC
^{89}Zr-DFO-SC16.56	RDC
^{177}Lu/^{225}Ac-MC339	RDC

Fig. 1 Overview of DLL3-targeting therapeutic strategies. (A) Diverse therapeutic modalities developed to engage the DLL3 pathway, including ADCs, TCEs, CAR-T, and RDCs; (B) chemical structures of the two lead peptide sequences, PepSP1171 and PepSP1214, which served as lead structures for optimization in this study.

their low immunogenicity minimizes immune-related adverse effects.[19–21] Considering the distinct pharmacokinetic properties of cyclic peptides relative to antibodies, the development of DLL3-targeting ligands based on cyclic peptides represents an important and promising research direction.

In this study, we selected two disclosed DLL3-binding peptide sequences, PepSP1171 and PepSP1214 (Fig. 1B),[22] previously patented by Amgen Inc., as lead scaffolds for optimization. Guided by molecular docking simulations, we first identified key residues likely involved in DLL3 interaction. Systematic amino acid substitutions and non-natural residue incorporations were then performed to investigate the initial structure-activity relationships (SAR) of the DLL3-targeting cyclic peptides.

Results and discussion

Design strategy guided by molecular dynamics and docking

Based on characterization data from the patent,[22] PepSP1171 and PepSP1214 were selected as lead scaffolds for structural modification due to their favorable binding affinity. For PepSP1171, an initial truncation of the C-terminal tail (residues AETVEFW) was evaluated. Molecular dynamics (MD)-based alanine scanning identified Gly4, Ser6, Asn8, Trp9, and Thr12 as structural hotspots ($\Delta\Delta G$ > 6 kJ mol^{-1}, Table S1), with Trp9 showing the greatest binding energy penalty ($\Delta\Delta G$ = 12.1 kJ mol^{-1}). Subsequent molecular docking of this core scaffold predicted a binding mode stabilized by a central anchoring module formed by the Trp9-Thr10 segment, which engages in multiple hydrogen bonds with Arg^{125} and Arg^{126} of DLL3 (Fig. 2A). Although molecular docking revealed no direct interaction between Gly4 and DLL3, its alanine mutation still caused a significant binding energy penalty ($\Delta\Delta G$ = 6.4 kJ mol^{-1}). Given its proximity to the binding interface, we propose that substitutions at Gly4 may modulate affinity by altering the backbone conformation. Based on these predictions, we started Gly4 and Trp9 for the initial optimization, while other hotspots (Ser6, Asn8, Thr12) were retained in this work for future optimization. At Gly4, we introduced conformationally constrained residues (cyclopropylalanine, cyclobutylalanine, or difluoromethylene-/olefinic-bridged groups) to reduce backbone flexibility and stabilize a high-affinity conformation. At Trp9, we incorporated aromatic non-natural amino acids (naphthyl, pyridyl, *p*-methylphenyl, *p*-methoxyphenyl, or biphenyl variants) to enhance hydrophobic complementarity and π-stacking within the binding pocket.

For PepSP1214, we adopted a conservative strategy that preserved the core cyclic structure while targeting tail sequence for fine-tuning. Val4 was selected for systematic optimization based on docking analysis, which showed its side chain projects into a hydrophobic pocket of DLL3 (Fig. 2B). We hypothesized that fine-tuning its size and conformation would enhance hydrophobic complementarity and stabilize the peptide in a more favorable binding pose.

It should be noted that, due to the flexibility of peptide ligands, docking and MD simulations may have limitations in predicting precise binding modes. Here, these methods were mainly used to guide peptide design, while SAR conclusions are primarily based on experimentally measured binding affinities.

Synthesis of cyclic peptides

Using a standard solid-phase peptide synthesis (SPPS) protocol on MBHA resin with the Fmoc protection strategy, the designed cyclic peptides **A1–A12** and **B1–B11** were successfully synthesized (Scheme 1). Each linear precursor contained cysteine (Cys) residues, whose thiol groups (–SH) underwent oxidative coupling in a DMSO/ACN system *via* air oxidation to form disulfide bonds (–S–S–), thereby achieving peptide cyclization. All final peptides were purified by reverse-phase high-performance liquid chromatography (RP-HPLC) to a purity greater than 95%, and their structural integrity was confirmed by mass spectrometry (MS) analysis (Table S2).

Binding affinities determination

The binding affinities of the synthesized cyclic peptides toward DLL3 were determined using biolayer interfer ometry (BLI) (Tables 1 and 2). Modification at the Trp9 position in PepSP1171 core scaffold revealed a clear structure–activity relationship. As shown in Table 1, only peptide **A4**, incorporating a 3-(1 naphthyl)-L-alanine substitution, exhibited strong binding affinity (K_D = 70 nM). We attribute this enhanced affinity to optimal π–π stacking interactions between the planar 1-naphthyl ring and Arg^{125}/Arg^{126} within the DLL3 binding pocket like the original indole ring. In contrast, substitutions with 3-(2-pyridyl)-L-

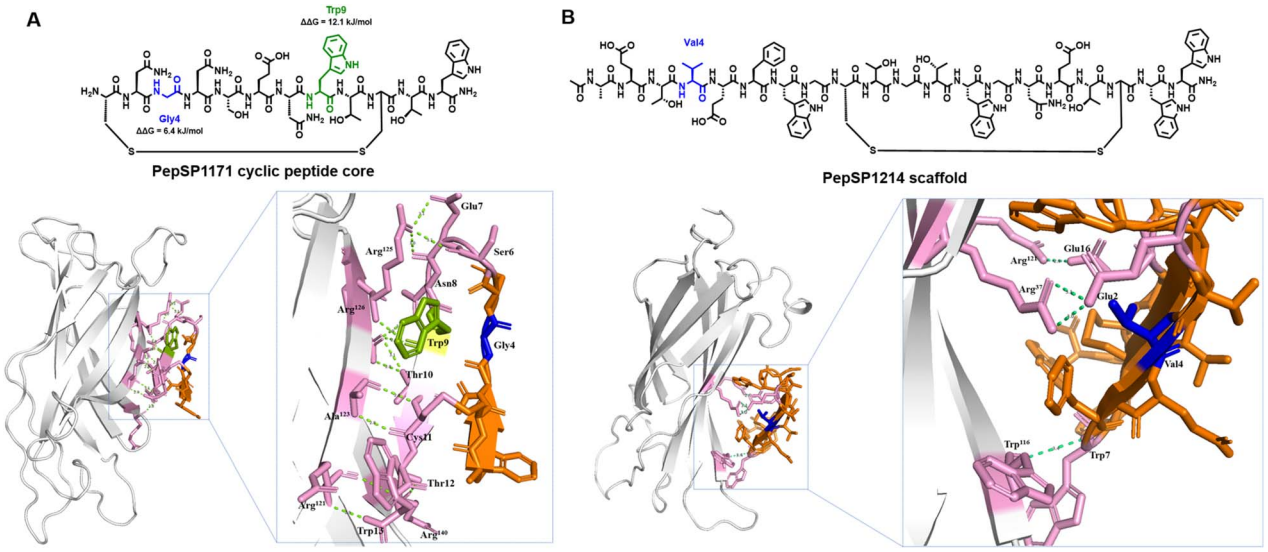

Fig. 2 Molecular docking model of the PepSP1171 cyclic peptide core (A) and PepSP1214 (B) with DLL3 using AlfaFold 3 (Gray represents DLL3 protein, orange represents peptide ligand, pink represents binding residues, and blue and green represent key modified sites).

alanine (**A1**), L-3-methylphenylalanine (**A2**) or L-3-methoxyphenylalanine replacements (**A3**) resulted in significantly weaker binding (K_D > 1000 nM), indicating that single aromatic ring system is disfavored. Furthermore, introducing a larger aromatic ring, such as diphenyl in **A5**, reduced affinity, highlighting steric constraints within the binding site.

Given the sensitivity of the Trp9 position, we retained the native indole ring and shifted our focus to the flexible Gly4 residue. Substitution with conformationally constrained analogues yielded a distinct activity profile. Peptides containing 1-aminocyclopropanecarboxylic acid (**A6**), 2-aminoisobutyric acid (**A7**), or 1-aminocyclobutanecarboxylic acid (**A8**) showed no detectable binding, likely due to introduced conformational

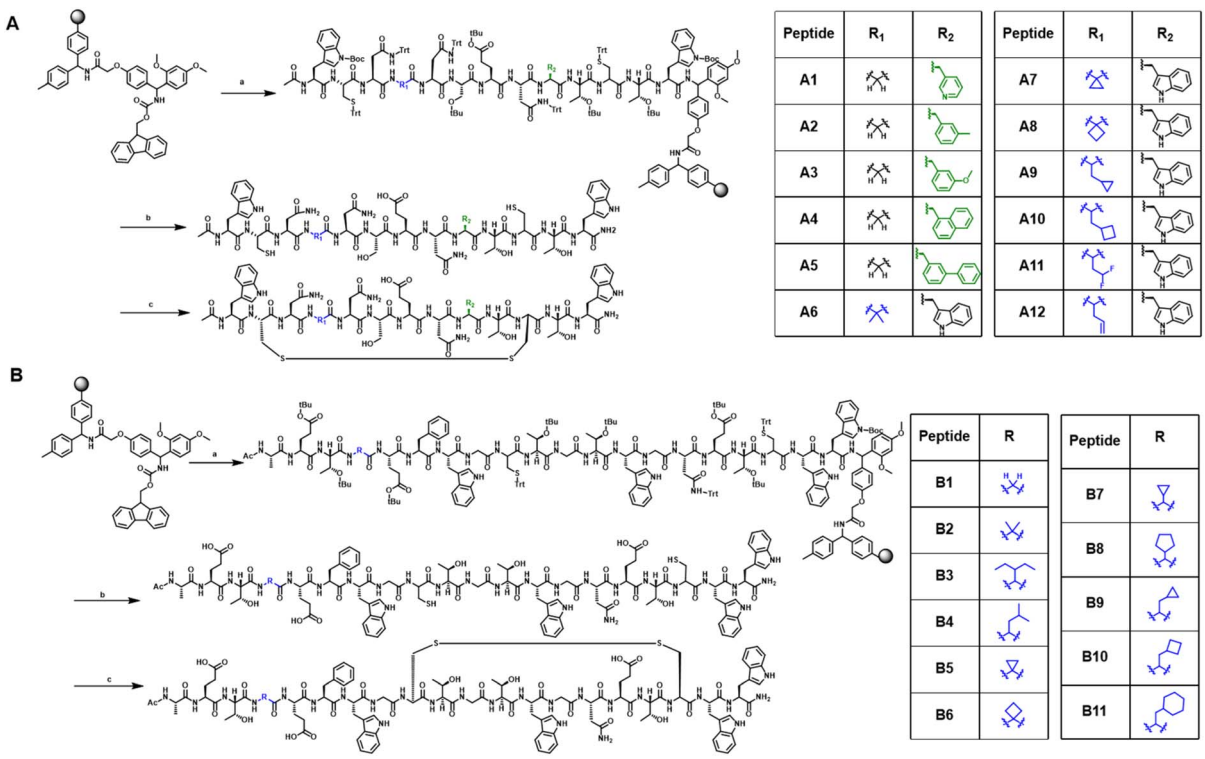

Peptide	R_1	R_2
A1		
A2		
A3		
A4		
A5		
A6		

Peptide	R_1	R_2
A7		
A8		
A9		
A10		
A11		
A12		

Peptide	R
B1	
B2	
B3	
B4	
B5	
B6	

Peptide	R
B7	
B8	
B9	
B10	
B11	

Scheme 1 Synthesis of designed DLL3-targeting peptides. (A and B) The synthetic routes for preparing the peptide libraries (**A1–A12**) and (**B1–B11**). Reaction and conditions: (a) DCM, DMF, piperidine, Fmoc-Amide, TBTU, DIEA; (b) 92.4%TFA, 2.5%TIS, 2.5%H_2O, 2.5%EDT, 0.1%TCEP, rt, 2 h; (c) ACN, DMSO, rt, 2 h.

Table 1 Structural information and binding affinities of the peptide analogues **A1–A12**[a]

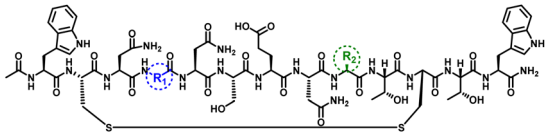

Peptide	R_1	R_2	K_D (nM)	k_a (1/Ms)	k_{dis} (1/s)
A1			>1000	1.02×10^4	6.22×10^{-2}
A2			>1000	1.23×10^4	1.60×10^{-1}
A3			>1000	2.98×10^8	1.96×10^1
A4			70	3.71×10^5	2.60×10^{-2}
A5		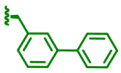	>1000	2.37×10^4	2.87×10^{-2}
A6			>1000	1.02×10^4	6.22×10^{-2}
A7			>1000	7.91×10^4	8.43×10^{-2}
A8			>1000	6.83×10^4	3.19×10^{-2}
A9			245	4.69×10^4	1.15×10^{-2}
A10			227	3.88×10^4	8.83×10^{-3}
A11			298	3.68×10^4	1.10×10^{-2}
A12			398	3.89×10^4	1.54×10^{-2}
PepSP1171			108	1.89×10^5	2.05×10^{-2}

[a] K_D values were determined using a BLI assay.

strain. However, more moderate constraints were partially tolerated. Peptides with cyclopropylalanine (**A9**, $K_D = 245$ nM), 2-amino-3-cyclobutylpropanoic acid (**A10**, $K_D = 227$ nM), 2-amino-4,4-difluorobutanoic acid (**A11**, $K_D = 298$ nM), or 2-aminobut-3-enoic acid (**A12**, $K_D = 398$ nM) retained measurable affinity, suggesting these groups can promote a binding-competent conformation. While these modifications on the core PepSP1171 scaffold provided us important structure–activity information, they did not yield ligands more potent than the lead peptide. This suggested that high-affinity binding requires interactions beyond the core structure, prompting a strategic shift to optimize the side chain for enhanced affinity.

Table 2 Structural information, analytical characterization, and binding affinity of the peptide analogues **B1–B11**[a]

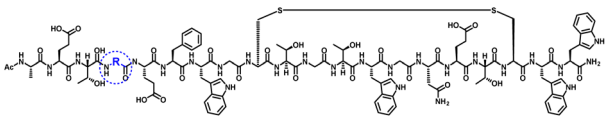

Peptide	R	K_D (nM)	k_a (1/Ms)	k_{dis} (1/s)
B1		449	3.02×10^4	1.36×10^{-2}
B2		668	1.91×10^4	1.27×10^{-2}
B3		80.5	7.59×10^4	6.11×10^{-3}
B4		270	5.68×10^4	1.54×10^{-2}
B5		12.3	1.37×10^5	1.69×10^{-3}
B6		150	9.06×10^4	1.36×10^{-2}
B7		93.1	7.73×10^4	7.19×10^{-3}
B8		180	4.82×10^4	8.69×10^{-3}
B9		91.7	1.05×10^5	9.61×10^{-3}
B10		72	1.18×10^5	8.52×10^{-3}
B11		357	3.82×10^4	1.36×10^{-2}
PepSP1214		180	4.82×10^4	8.69×10^{-3}

[a] K_D values were determined using a BLI assay.

Our optimization of PepSP1214 focused on the Val4 position, where valine was systematically replaced with natural and non-natural amino acids. Analysis of the resulting peptides (**B1–B11**, Table 2) revealed that the most potent

binder was peptide **B5**, which incorporates the rigid 1-aminocyclopropane-1-carboxylic acid and exhibits a high binding affinity for DLL3 (K_D = 12.3 nM). This represents a great improvement over the native valine side chain and suggests that the cyclopropyl group possibly achieves an optimal, tight fit within a hydrophobic pocket of DLL3. Further analysis of cyclic substituents revealed a clear size dependence. Enlarging the ring to a cyclobutyl group (**B6**, K_D = 150 nM; **B10**, K_D = 72 nM) or incorporating a cyclopropyl group with an extended methylene linker (**B9**, K_D = 91.7 nM; **B7**, K_D = 93.1 nM) resulted in good, but reduced, affinity compared to **B5**. This indicates that the pocket has limited volume and favors small, compact hydrophobic groups. The significant drop in affinity observed with the large cyclohexyl substituent in **B11** (K_D = 357 nM) confirms the steric constraints of the binding site.

The highly branched 2-amino-2-methylpropanoic acid in **B2** (K_D = 668 nM) and the flexible, short-chain glycine in **B1** (K_D = 449 nM) led to the greatest loss of binding. In contrast, a linear side chain with moderate length and flexibility, as in 2-amino-3-ethylpentanoic acid (**B3**, K_D = 80.5 nM), was well-tolerated, supporting the role of hydrophobic interactions without strict conformational constraints.

According to the above results, we found that the Val4 position is highly sensitive to modification. The superior performance of the cyclopropyl group in **B5** establishes that small size, high rigidity, and optimal hydrophobic packing are the key factors for enhancing binding affinity at this site.

In summary, a rational design strategy focusing on three key sites, Trp9 and Gly4 of PepSP1171 core and Val4 of PepSP1214, successfully improved the affinity of DLL3-targeting cyclic peptides. This optimization yielded six peptides with high binding affinity (K_D < 100 nM; see representative binding kinetic curves in Fig. S1) and established an initial structure–activity relationship (SAR). The SAR revealed distinct structural requirements: the Trp9 position favored optimal π–π stacking, achieved with 3-(1-naphthyl)-L-alanine (**A4**, K_D = 70 nM), while the Gly4 position required conformational size compatible. The most significant improvement came from modifying Val4 on PepSP1214, where substituting valine with small, rigid 1-aminocyclopropane-1-carboxylic acid produced peptide **B5** with a K_D of 12.3 nM. These results demonstrate the success of our structure-based approach in developing high-affinity DLL3 binders.

Conclusions

In conclusion, we have successfully designed and synthesized 23 new cyclic peptides targeting DLL3. Our structure-based optimization strategy successfully identified peptide **B5**, which incorporates a rigid 1-aminocyclopropane-1-carboxylic acid substitution and achieves improved affinity (K_D = 12.3 nM). This work validates our rational design approach and establishes peptide **B5** as a promising lead candidate for the further development of targeted radiotracers, peptide-drug conjugates, and other theranostic agents for the treatment of SCLC and related malignancies.

Experimental section

Procedure for the preparation of cyclic peptides

All cyclic peptides were synthesized on MBHA resin (0.57 mmol g^{-1} loading capacity) using standard Fmoc solid-phase peptide synthesis (SPPS). General procedure: MBHA resin (0.35 g, 0.2 mmol) was swollen in dichloromethane (DCM, 15 mL) at room temperature for 15 min and then washed three times with *N*,*N*-dimethylformamide (DMF). Fmoc deprotection was performed by treating the resin with 10 mL of piperidine-DMF (1 : 4, v/v) at room temperature for 5 min, followed by draining and repeating the treatment for an additional 10 min. The resin was subsequently washed six times with DMF. Successful Fmoc removal was confirmed by a ninhydrin test, which produced a deep blue color after heating at 110 °C for 3 min. For the coupling step, Fmoc-Trp(Boc)-OH (320 mg, 3 equiv.) and TBTU (193 mg, 3 equiv.) were dissolved in DMF, and *N*,*N*-diisopropylethylamine (DIEA, 0.208 mL, 6 equiv.) was added under an ice bath for pre-activation (10 min). The activated mixture was added to the deprotected resin and allowed to react at room temperature for 1 h. Completion of the coupling reaction was confirmed by a negative ninhydrin test (colorless result). The resin was then washed three times with DMF. Fmoc deprotection and coupling cycles were repeated until the full peptide sequence was assembled. Subsequently, the terminal amine was acetylated using Ac_2O (56 μL, 3 equiv.) and DIEA (209 μL, 6 equiv.). The resin was washed alternately three times with DCM and ethanol (10 mL each) and vacuum-dried at 35 °C for 2 h. Peptide cleavage was performed by adding a cleavage cocktail (TFA : TIS : H_2O : EDT = 92.4 : 2.5 : 2.5 : 2.5, v/v) containing TCEP (9 mg) at a ratio of 10 mL g^{-1} resin. The mixture was stirred at room temperature for 2 h. The filtrate was slowly added dropwise into cold methyl *tert*-butyl ether (MTBE, 50 mL) and allowed to precipitate in an ice bath for 1 h. The precipitate was collected by centrifugation, washed three times with MTBE, and dried at 35 °C to yield the crude peptide. The crude product was dissolved in NH_4OAc buffer (52 mL, pH = 9) and mixed with acetonitrile (52 mL) and dimethyl sulfoxide (DMSO, 5.5 mL). The solution was stirred at room temperature for 2 h. Completion of the reaction was confirmed by LC-MS analysis. The desired peptide was obtained after purification by preparative HPLC, followed by concentration and lyophilization. The molecular weights of the products were confirmed by ESI-MS. The mobile phases consisted of 0.1% TFA in water (A) and 0.1% TFA in acetonitrile (B). The following gradient was then applied at a flow rate of 1.0 mL min^{-1}: 5% B (0–5 min), raised to 26% B (5–7 min), and further to 36% B (7–27 min). Detailed analytical data (including HPLC chromatograms and mass spectra) are provided in the SI.

BLI binding assays

The dynamic binding affinity between peptide compounds and the target protein was characterized using BLI on an Octet R8 instrument (Sartorius, Germany). The target protein was biotinylated recombinant human DLL3 (Acro Biosystems Inc., catalog no. DL3-H82Ea). Briefly, DLL3 protein was diluted to 20 μg mL^{-1} in PBST and immobilized onto streptavidin (SSA) biosensors. The peptide compounds were then diluted to five appropriate

concentrations in PBST containing ≤1% DMSO for affinity measurement, while blank SSA sensors without immobilized protein were tested in parallel to correct for non-specific binding. After the assay, sensorgram data were analyzed using Octet Analysis Studio (version 12.2.2.26), and the kinetic parameters were obtained by global fitting to a 1 : 1 binding model to calculate the association rate constant (k_a), dissociation rate constant (k_{dis}), and equilibrium dissociation constant (K_D).

Author contributions

All authors have reviewed and approved the final version of the manuscript. The individual contributions are as follows: Xinyan Gao performed peptide synthesis and data analysis, and drafted the manuscript; Xiaochuan Zha conducted and analyzed the molecular dynamics and docking simulations; Wenhao Liu and Jiale Xie contributed to peptide synthesis; Jian Gao provided conceptual guidance and reviewed the manuscript; Zonghua Luo oversaw project administration, acquired funding, provided conceptual guidance, and contributed to manuscript review and editing.

Conflicts of interest

There are no conflicts to declare.

Data availability

The data supporting this article have been included as part of the supplementary information (SI). Supplementary information: Tables S1 and S2, BLI binding kinetics curves (Fig. S1), and HPLC/MS spectra. See DOI: https://doi.org/10.1039/d6ra02966c.

Acknowledgements

This research was funded by the Faculty Start-up Foundation of ShanghaiTech University (grant number 2021F0209-000-04).

Notes and references

1 J. W. Kim, J. H. Ko and J. Sage, *iScience*, 2022, **25**, 105603.
2 D. L. Cortinovis, F. Colonese, M. I. Abbate, L. Sala, M. Meazza Prina, N. Cordani, E. Sala and S. Canova, *Front. Med.*, 2022, **9**, 989405.
3 B. Zhou, W. Lin, Y. Long, Y. Yang, H. Zhang, K. Wu and Q. Chu, *Signal Transduct. Target. Ther.*, 2022, **7**, 95.
4 M. Furuta, H. Kikuchi, T. Shoji, Y. Takashima, E. Kikuchi, J. Kikuchi, I. Kinoshita, H. Dosaka-Akita and J. Sakakibara-Konishi, *Cancer Sci.*, 2019, **110**, 1599–1608.
5 M. Shirasawa, T. Yoshida, K. Shiraishi, N. Goto, S. Yagishita, T. Imabayashi, Y. Matsumoto, K. Masuda, Y. Shinno, Y. Okuma, Y. Goto, H. Horinouchi, M. Yotsukura, Y. Yoshida, K. Nakagawa, K. Naoki, T. Tsuchida, R. Hamamoto, N. Yamamoto, N. Motoi, T. Kohno, S. Watanabe and Y. Ohe, *Br. J. Cancer*, 2023, **129**, 2003–2013.
6 C. M. Rudin, M. Reck, M. L. Johnson, F. Blackhall, C. L. Hann, J. C.-H. Yang, J. M. Bailis, G. Bebb, A. Goldrick, J. Umejiego and L. Paz-Ares, *J. Hematol. Oncol.*, 2023, **16**, 66.
7 P.-L. Su, K. Chakravarthy, N. Furuya, J. Brownstein, J. Yu, M. Long, D. Carbone, Z. Li and K. He, *Mol. Cancer*, 2024, **23**, 97.
8 H. Wang, T. Zheng, D. Xu, C. Sun, D. Huang and X. Liu, *Pharmaceutics*, 2025, **17**, 520.
9 J. Ding and C. Yeong, *Front. Oncol.*, 2024, **14**, 1504139.
10 A. S. Mansfield, D. S. Hong, C. L. Hann, A. F. Farago, H. Beltran, S. N. Waqar, A. E. Hendifar, L. B. Anthony, M. H. Taylor, A. H. Bryce, S. T. Tagawa, K. Lewis, J. Niu, C. H. Chung, J. M. Cleary, M. Rossi, C. Ludwig, R. Valenzuela, Y. Luo and R. Aggarwal, *Npj Precis. Oncol.*, 2021, **5**, 74.
11 M. R. Patel, Y. Sun, H. Wang, W. Yao, L. G. Paz-Ares, Y. Fu, X. Liu, X. Wang, R. Zhou and J. Zhao, *J. Clin. Oncol.*, 2025, **43**, 3041.
12 Q. Guo, B. Gao, R. Song, W. Li, S. Zhu, Q. Xie, S. Lou, L. Wang, J. Shen, T. Zhao, Y. Zhang, J. Wu, W. Lu and T. Yang, *Mol. Cancer Ther.*, 2024, **23**, 1367–1377.
13 M. J. Giffin, K. Cooke, E. K. Lobenhofer, J. Estrada, J. Zhan, P. Deegen, M. Thomas, C. M. Murawsky, J. Werner, S. Liu, F. Lee, O. Homann, M. Friedrich, J. T. Pearson, T. Raum, Y. Yang, S. Caenepeel, J. Stevens, P. J. Beltran, J. Canon, A. Coxon, J. M. Bailis and P. E. Hughes, *Clin. Cancer Res.*, 2021, **27**, 1526–1537.
14 L. Paz-Ares, S. Champiat, W. V. Lai, H. Izumi, R. Govindan, M. Boyer, H.-D. Hummel, H. Borghaei, M. L. Johnson, N. Steeghs, F. Blackhall, A. Dowlati, N. Reguart, T. Yoshida, K. He, S. M. Gadgeel, E. Felip, Y. Zhang, A. Pati, M. Minocha, S. Mukherjee, A. Goldrick, D. Nagorsen, N. Hashemi Sadraei and T. K. Owonikoko, *J. Clin. Oncol.*, 2023, **41**, 2893–2903.
15 D. Zhou, L. A. Byers, B. Sable, M. D. Smit, N. H. Sadraei, S. Dutta and V. V. Upreti, *J. Clin. Pharmacol.*, 2024, **64**, 362–370.
16 K. M. Tully, S. Tendler, L. M. Carter, S. K. Sharma, Z. V. Samuels, K. Mandleywala, J. A. Korsen, A. M. Delos Reyes, A. Piersigilli, W. D. Travis, T. Sen, N. Pillarsetty, J. T. Poirier, C. M. Rudin and J. S. Lewis, *Clin. Cancer Res.*, 2022, **28**, 1391–1401.
17 S. Tendler, M. P. Dunphy, M. Agee, J. O'Donoghue, R. G. Aly, N. J. Choudhury, A. Kesner, A. Kirov, A. Mauguen, M. K. Baine, H. Schoder, W. A. Weber, N. Rekhtman, S. K. Lyashchenko, L. Bodei, M. J. Morris, J. S. Lewis, C. M. Rudin and J. T. Poirier, *Lancet Oncol.*, 2024, **25**, 1015–1024.
18 A. Savinainen, L. Wu, T. Bruton, A. Chonkar, J. Cupido, J. Dearling, C. Huang, K. Lee, Z. Ma, H. Mok, K. Nabi, A. Salih, A. Sutton, L. Tavera, M. Wan, Z. Wang, X. Xu, J. Xu, A. Zidell and A. Ricardo, *Ann. Oncol.*, 2024, **35**, S755.
19 D. Wang, F. Yin, Z. Li, Y. Zhang and C. Shi, *J. Nanobiotechnology*, 2025, **23**, 305.
20 T. T. Dean, J. Jelú-Reyes, A. C. Allen and T. W. Moore, *J. Med. Chem.*, 2024, **67**, 1641–1661.
21 K. Sharma, K. K. Sharma, A. Sharma and R. Jain, *Drug Discov. Today*, 2023, **28**, 103464.
22 J. Bailis, S. A. M. Tiso and M. Salvati, *China Pat.*, CN 118434754A, 2024.